Elastic scattering of ^{8}He + ^{4}He and two-neutron transfer and the influence of resonances in ^{12}Be

M. Freer, N.I. Ashwood, N.L. Achouri, W.N. Catford, N. Curtis, F. Delaunay, H. Al Falou, F.M. Marqués, T. Munoz-Britton, N.A. Orr, et al.

Physics Letters B 775 (2017) 58–62

Contents lists available at ScienceDirect

Physics Letters B

www.elsevier.com/locate/physletb

Elastic scattering of ^{8}He + ^{4}He and two-neutron transfer and the influence of resonances in ^{12}Be

M. Freer [a,*], N.I. Ashwood [a], N.L. Achouri [b], W.N. Catford [c], N. Curtis [a], F. Delaunay [b], H. Al Falou [b,1], F.M. Marqués [b], T. Munoz-Britton [a], N.A. Orr [b], R. Raabe [d,2], N. Soić [e], J.S. Thomas [c], C. Wheldon [a], V.A. Ziman [a]

[a] School of Physics and Astronomy, University of Birmingham, Edgbaston, Birmingham, B15 2TT, UK
[b] LPC Caen, ENSICAEN, Université de Caen, CNRS/IN2P3, Caen, France
[c] School of Electronics and Physical Sciences, University of Surrey, Guildford, Surrey, GU2 7XH, UK
[d] GANIL, Boulevard Henri Becquerel, 14000 Caen, France
[e] Rudjer Bošković Institute, Department of Experimental Physics, Bijenička 54, HR-10000 Zagreb, Croatia

ARTICLE INFO

Article history:
Received 25 August 2017
Received in revised form 7 October 2017
Accepted 25 October 2017
Available online 27 October 2017
Editor: V. Metag

Keywords:
Nuclear clustering
Molecular states
Light nuclei

ABSTRACT

Scattering of ^{8}He from ^{4}He has been performed through the coincident detection of the scattered particles using a silicon array within a helium-4 gas volume with a ^{8}He beam. This permitted the reconstruction of the interaction probability as a function of position within the gas and hence the excitation function to be calculated together with the angular distribution of the products. These measurements also enabled the reconstruction of the two-neutron transfer to ^{6}He + ^{6}He. The measurements provide the first characterisation of the scattering of the $\alpha + 4n$, ^{8}He, halo nucleus from ^{4}He and the $2n$-transfer to populate the symmetric final state. The results indicate the presence of a $L = 4$ component at excitation energies of 14–15 MeV, consistent with a broad ($\sim$ 1 MeV) $J^{\pi} = 4^{+}$ resonance. These measurements would agree with generalized two-centre cluster model (GTCM) calculations indicating a cluster, or molecular, structure predicted at this energy.

The possibility that nuclei can mimic atomic systems is an intriguing one. In covalently bound atomic systems electrons are exchanged in delocalized orbits. It has been suggested [1] that for the beryllium isotopes the exchange of valence neutrons between α-particle cores may occur in a similar fashion. Indeed, in the case of ^{9}Be the ground-state ($J^{\pi} = 3/2^{-}$) and first excited $1/2^{+}$ states possess rotational bands which may be characterised in terms of π and σ-covalent orbitals [1]. The most dramatic example comes from the characterisation of the excited states of ^{10}Be, where two neutrons in σ-orbits reside between the α-particles and, owing to the Pauli Exclusion Principle, increase the separation of the α-particles to form perhaps the most deformed nuclear state presently known [2].

The case of the even more exotic ^{12}Be has yet to be resolved; here 4 neutrons can be covalently exchanged. Even in the ground-state the $N = 8$ shell closure is broken, with the state being deformed due to the presence of clustering [3,4]. The earliest measurements of inelastic breakup of ^{12}Be [5,6] observed a series of states (albeit with limited statistics) that decayed into ^{6}He + ^{6}He and ^{4}He + ^{8}He. The angular correlation studies had suggested possible spin assignments [6]. Later measurements [7] found evidence for some of these states, though the agreement was only partial and the states appeared to be quite broad (1 MeV). Most recently a measurement of the ^{12}C(^{12}Be,^{6}He + ^{6}He) reaction has been performed at IMP-Lanzhou [8] that identified additional lower energy states with potential molecular character.

From the theoretical perspective there is some guidance as to the structures expected above the ^{6}He and ^{4}He decay thresholds in ^{12}Be of 10.1 and 8.9 MeV, respectively. In particular, the two-centre cluster model calculations of Ito et al. [9,10] provide a strong basis for the interpretation of resonances in this region in terms of their molecular, or cluster, behaviour. These calculations simulate the scattering of ^{8}He from ^{4}He and include the influence of the cluster and molecular states in ^{12}Be. The challenge is to provide

* Corresponding author.
E-mail address: M.Freer@bham.ac.uk (M. Freer).
[1] *Present address:* Université de Technologie et de Sciences Appliquées Libano-Française, Tripoli, Lebanon.
[2] *Present address:* KU Leuven, Instituut voor Kern-en Stralingsfysica, Celestijnenlaan 200D, 3001 Leuven, Belgium.

https://doi.org/10.1016/j.physletb.2017.10.063

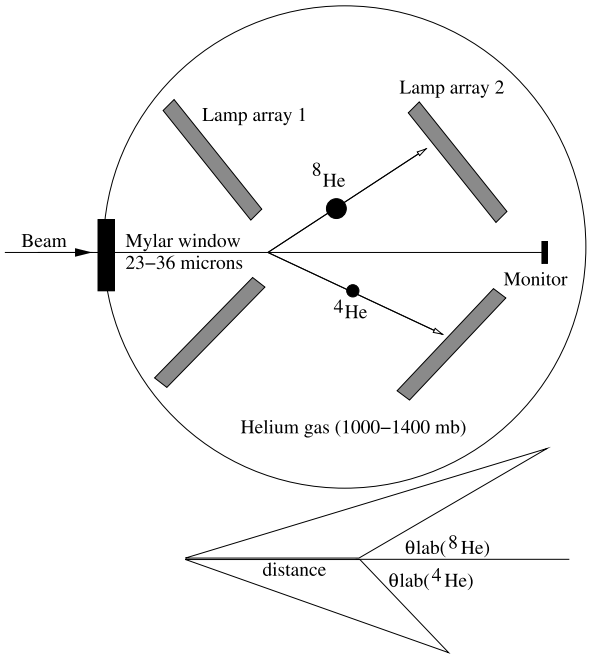

Fig. 1. Experimental setup.

further experimental evidence for the influence of such resonances in the excitation energy region in which the molecular resonances are predicted.

Here we present measurements of the ^{8}He + ^{4}He elastic scattering and the 2n transfer reaction in which we identify potential resonant contributions and characterise the spin of one of the ^{12}Be resonances. These measurements involve a low intensity ^{8}He beam and a gas target at the limit of the experimental technique. Moreover, they provide a precision measurement of the elastic scattering angular distributions and the two-neutron transfer cross section. This reaction is of particular interest as in atomic systems two-electron transfer or exchange through the influence of covalent orbitals has been demonstrated to have a strong influence on the energy dependence of the atomic scattering reaction [11]. The present system, as illustrated by the two-centre cluster model calculations of Ito et al. [9,10], is a direct analogue of the atomic system. Moreover, these data provide an interesting test of the scattering of the $\alpha + 4n$, ^{8}He, halo nucleus from a target which is the halo core.

A pure ^{8}He ($T_{1/2} = 119$ ms) beam was produced by the SPIRAL facility at GANIL with an intensity of $5–6 \times 10^4$ pps. Beams of energies 20 and 24 MeV transited a Mylar foil window into the ECLAN reaction chamber which was filled with high purity helium-4 gas maintained at pressures between 1000 and 1400 mbar. Two Mylar windows of thickness 23 μm and 36 μm were used to vary the incident beam energy. The energy loss of the beam through the windows was, for the 20 MeV beam, 1.73 MeV and 2.76 MeV for the thin and thick windows respectively, and for the 24 MeV beam 1.49 MeV and 2.37 MeV. As the ^{8}He energy loss within the gas is relatively small and the experimental gas pressure was limited to 1400 mbar this variety of measurements were required in order to probe a sufficiently large range of ^{12}Be excitation energies.

The experimental arrangement was very similar to that deployed in Ref. [12] and is shown in Fig. 1. Within the gas volume there were two arrays of large-area, segmented, silicon detectors composed of YY1 wedge shaped detectors [13], which were 500 μm thick. Each array was formed from 6 detectors in a "lampshade" type configuration [14]. Two such lampshade arrays, Lamp1 and Lamp2, were arranged within the gas at 15.0(5) and 25.5(5) cm from the window. The inclination of these detectors from the beam axis was 46°. The detectors covered angles, measured with respect to the window, of 13.0 to 39.0° (Lamp1) and 7.5 to 21.0° (Lamp2). Beyond the two lampshade detector arrays was a small (2 cm diameter) silicon monitor detector which was used to record the integrated number of beam particles – the range of ^{8}He at energies close to 20 MeV and the present gas pressures is in excess of 1 m. The energy resolution averaged over all of the strips of the silicon detectors was $\sim$ 150 keV (FWHM). Four combinations of beam energies, window thicknesses and gas pressures were used; i) 24 MeV, 23 μm, 1000 mbar, ii) 24 MeV, 36 μm, 1000 mbar, iii) 20 MeV, 36 μm, 1400 mbar and iv) 20 MeV, 23 μm, 1200 mbar. The data were normalized through the integrated yield in the monitor. This was cross checked against the calculated beam exposure and an analysis of scattering from the chamber entrance window into the Lamp detectors. From this comparison the uncertainty in the normalisation is, in the worst case, 30%. This uncertainty is reflected in the yields shown in Fig. 4. The main issue with the beam normalisation is that the multiple scattering of the beam in the gas resulted in only a fraction of the beam being incident on the zero degree monitor.

As the beam passes through the gas volume covered by the silicon array, losing energy through collisions with the gas, it traces out an excitation function, i.e. the energy within the centre-of-mass (c.m.) frame varies with the location in the chamber. This also means that the equivalent energy of the composite, ^{12}Be, system is varying. The energy loss over the path length imaged by the detectors (25 cm path length for singles detection events and 19 cm for coincidences) is typically small, $\sim$ 2.5 MeV, which corresponds to a variation in the c.m. frame of only $\sim$ 830 keV. The present set of measurements sample the ^{12}Be excitation energy range 13.7 to 16.4 MeV.

The approach used to reconstruct the events of interest was to detect the elastically scattered ^{4}He and ^{8}He in coincidence on opposing sides of the beam axis. Such events were clearly identified by plotting the detected energy of one particle against that of the other. For elastic scattering energy is conserved. Reactions involving inelastic scattering to the ^{8}He first excited state, which is unbound to neutron decay, lead to a four-body final state which washes out the kinematics and hence cannot be clearly distinguished. Conversely, two-neutron transfer to produce ^{6}He + ^{6}He ($Q = -1.17$ MeV) may also be observed as a 2-body coincidence. Coincidences were possible between all of the Lampshade detectors, i.e. 1-1, 1-2 and 2-2 (e.g. a 2-2 coincidence is shown in Fig. 1).

By initially assuming an average interaction point it was possible to estimate the c.m. energy for the ^{4}He − ^{8}He system. Assuming the first detected particle was ^{4}He and the second ^{8}He, an energy loss incurred by the particles in traversing the gas from reaction to detection point was used to correct the detected energy. In turn, the corrected energies of the ^{4}He − ^{8}He nuclei and the assumed c.m. reaction energy may be used to calculate the c.m. angles and the laboratory emission angles for both particles. For correctly identified coincidences and assumed particle masses (there is no explicit particle identification) the c.m. angles sum to 180°. This was then used as an event selection criteria.

Further, as shown in Fig. 1, it is possible to use the laboratory scattering angles, calculated in this manner, and the angle and distance of the strip measured from the window, θ_w, to calculate the distance at which the reaction takes place from the window, d_w. This may be calculated for both particles – and then compared. This analysis is presented in Fig. 2. The distance from the window, d, can be calculated from the reaction kinematics and the measured particle velocity (for particle 1, m_1, with complementary particle m_2), v_{1lab}, the angle of the particle measured from the

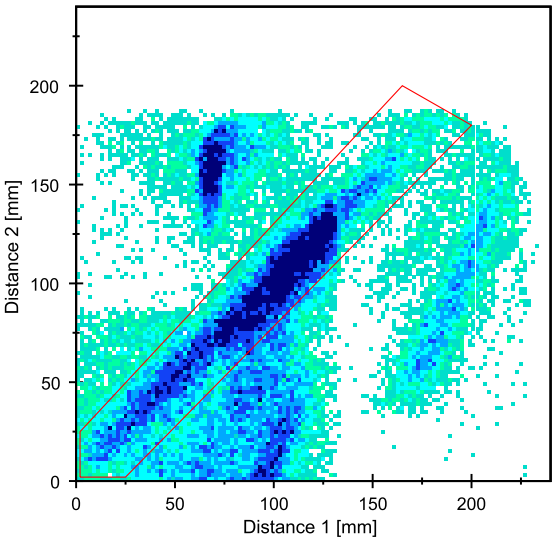

Fig. 2. (Colour online.) The interaction distance calculated for the two detected particles. Events on the diagonal correspond to the correct identification of the two particles as $1 = {}^4$He and $2 = {}^8$He (selected using the gate shown). Events where the identification is incorrect, i.e. $2 = {}^4$He and $1 = {}^8$He lie away from the diagonal. The data are for: $E_{beam} = 24$ MeV, window thickness 36 μm and gas pressure 1000 mbar.

window, θ_{1w}, and the distance of that detector element from the window, d_{1w}:

$$v_{1cm} = \sqrt{\frac{2m_2 E_{beam}}{(m_1 + m_2)^2}}, \tag{1}$$

$$\theta_{1lab} = \cos^{-1}\left(\frac{v_{cm}^2 + v_{1lab}^2 - v_{1cm}^2}{2v_{cm}v_{1lab}}\right), \tag{2}$$

and

$$d_1 = d_{1w}\frac{\sin(\theta_{1lab} - \theta_{1w})}{\sin(\pi - \theta_{1lab})}. \tag{3}$$

Here E_{beam} is the beam energy and v_{cm} is the centre-of-mass velocity. The centre-of-mass emission angle follows as

$$\theta_{1cm} = \cos^{-1}\left(\frac{v_{1cm}^2 + v_{cm}^2 - v_{1lab}^2}{2v_{cm}v_{1cm}}\right). \tag{4}$$

Events in which the detected particles masses have been correctly identified as $1 = {}^4$He and $2 = {}^8$He lie on the diagonal and are selected by the gate shown (red box). Those events lying outside the window were then assumed to be particle $1 = {}^8$He and $2 = {}^4$He and the analysis repeated, with again correctly identified events selected by the gate shown.

For events selected in the above manner, it was possible to plot the average distance, $d = (d_1 + d_2)/2$, at which the reaction took place in the chamber against the average c.m. angle (calculated from the values determined from the coincident particles). Note that the distance is equivalent to the excitation energy, with the highest excitation energy corresponding to smaller distances. Two examples of such plots are shown in Fig. 3. The experimental data (left panels) show three broad regions as a function of distance from the window (0 being the window). Coincident events with both particles in Lamp1 lie in the region between 0 and 80 mm. At about 100 mm the particles are detected separately in Lamp1 and Lamp2 and then at distances larger than 125 mm the two particles are detected in Lamp2 (as illustrated in Fig. 1).

Fig. 3 also shows the results of simulations assuming isotropic angular and energy distributions and including the energy losses

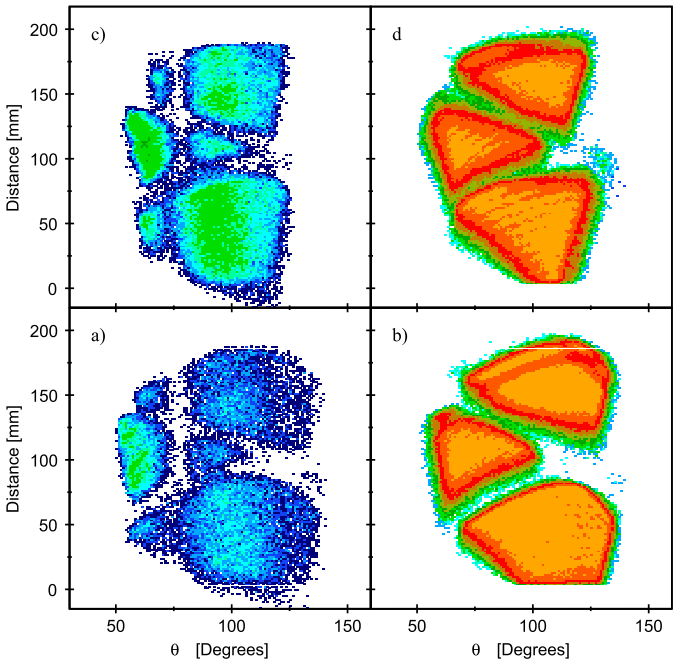

Fig. 3. (Colour online.) Average distance plotted against the average centre-of-mass angle of the ^{4}He nucleus (θ_{cm}), for the parameters a) $E_{beam} = 24$ MeV, window thickness 36 μm and gas pressure 1000 mbar and c) $E_{beam} = 20$ MeV, window thickness 23 μm and gas pressure 1200 mbar. Plots b) and d) are the simulations of a) and c), respectively.

and detection processes, which show the acceptances expected for the measurements. These simulations also include the missing strips which may be seen (reduced efficiency) to produce features in the data at large distances. The Monte Carlo simulations show that it would have been possible to reconstruct resonances with a width of 50 keV. Hence it can be concluded that within the energy range sampled the data show *no* indication of narrow, 50–100 keV, resonances. It may be noted that the data exhibit a deficit of counts with respect to the simulations most notably at $\theta_{cm}({}^4\text{He}) = 75°$. This is due to a minimum in the angular distributions associated with the $^8\text{He} + {}^4\text{He}$ scattering (see below).

The data integrated over the centre-of-mass angular range 80–120° (the region of the maximum in the angular distributions), normalized by the beam exposure and the calculated detection efficiency, is shown in Fig. 4. The error bars here reflect the uncertainty in the beam normalisation described earlier. There are 12 data points for the $^8\text{He} + {}^4\text{He}$ data corresponding to the 4 different experimental configurations and the three regions seen in Fig. 3. For the $^6\text{He} + {}^6\text{He}$ channel there are only 4 data points as only one of the regions in Fig. 3 could be analysed due to the high backgrounds in the other two (see later). Note that it was difficult to calculate total cross sections for the yield as this requires an extrapolation beyond the present angular range. Hence only the differential cross sections are presented in Figs. 5 and 6. The experimental angular distributions provide a strong characterisation of both the elastic $2n$ transfer reactions, which may be used to constrain reaction model calculations of this exotic system. Here, though, we focus on the potential resonant behaviour of the $^8\text{He} + {}^4\text{He}$ reaction.

The data in Fig. 4 have been compared with a line-shape for two resonances at 13 and 15 MeV, with widths of 1 MeV and amplitudes to match that found for the $^8\text{He} + {}^4\text{He}$ channel in Ref. [7]. The data are consistent with the peaks observed in the earlier measurements [6,7], which identified resonances at 12.8 and 15.5 MeV [7], though would indicate the latter peak lies closer

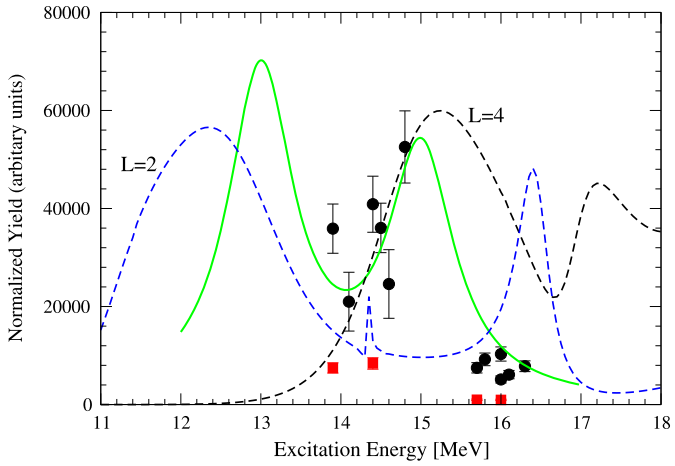

Fig. 4. (Colour online.) The experimental yields, corrected for the detection efficiency, for the ^{8}He + ^{4}He reaction (black circles) and ^{6}He + ^{6}He reaction (red squares) compared with resonance profiles with two non-interfering resonances at 13 and 15 MeV (see text) with widths (Γ) of 1 MeV (solid-green line). The $L = 2$ (blue-dashed line) and $L = 4$ (black-dashed line) strength from the GTCM calculations are shown [10].

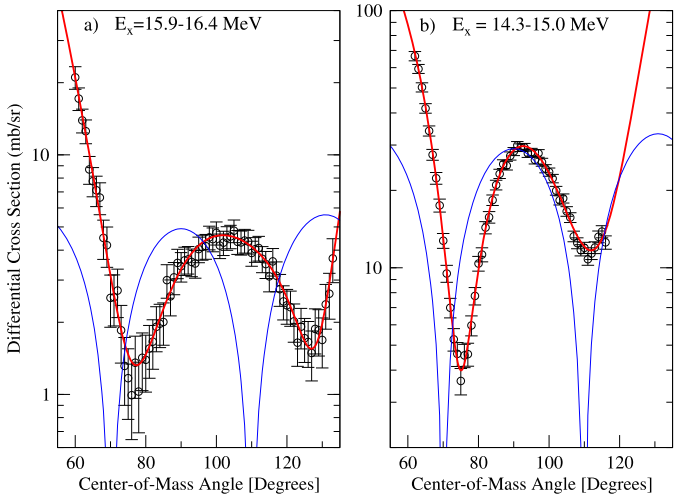

Fig. 5. (Colour online.) Angular distributions for the ^{4}He(^{8}He,^{4}He)^{8}He elastic scattering reaction for the excitation energy ranges a) 15.9–16.4 MeV and b) 14.3–15.0 MeV. The fit (red-line) corresponds to the functional form given in Eq. (5) with $L_{max} = 4$. Uncertainties in the amplitudes are typically 0.3. The blue lines correspond to $|P_4(\cos(\theta_{cm})|^2$ distributions. The lower energy data follow more closely the trend of the $L = 4$ Legendre polynomial.

to 15 MeV. However, it should be noted that the present measurements strictly only demonstrate enhanced yield at the lower energy compared with the higher c.m. energy.

The angular distributions for the excitation-energy intervals 14.3–15.0 MeV and 15.9–16.4 MeV are shown in Fig. 5. The uncertainties shown are statistical uncertainties and the uncertainty in the absolute value of the differential cross section is expected to be up to 30%. The angular distributions, as revealed in Fig. 3, display a diffractive behaviour with a deep minimum at $\theta_{cm} \simeq 75°$. What is also noticeable is that the maximum in the centre of the experimental acceptance shifts to smaller angles for the lower beam energy (Fig. 3c) compared to the higher beam energy (Fig. 3a).

Following an approach which is similar to the phase shift analysis performed for ^{4}He + ^{4}He elastic scattering data [15], these ^{4}He + ^{8}He elastic scattering data have been fitted with a partial wave analysis

Table 1
The values of χ^2/dof for the fits as a function of the maximum angular momentum, L_{max}, of the fits to the data shown in Fig. 5.

Excitation energy (MeV)	$L_{max} = 2$	$L_{max} = 3$	$L_{max} = 4$	$L_{max} = 5$
14.3–15.0	6.1	6.3	1.4	1.4
15.9–16.4	2.4	0.8	0.8	0.7

Table 2
The amplitudes, a_L, used in the fit of the angular distributions shown in Fig. 5 and used in Eq. (5) at the lower and higher excitation energies. The ratios of the amplitudes at the two energies are also given.

Excitation energy (MeV)	$L = 0$	$L = 1$	$L = 2$	$L = 3$	$L = 4$
14.3–15.0	5.89	25.03	17.42	12.86	21.11
15.9–16.4	5.48	14.64	13.08	12.28	8.78
Ratio	1.07	1.71	1.33	1.05	2.41

$$W(\theta) = \left| \sum_{L=0}^{L_{max}} a_L e^{i\varphi_L} P_L(\cos\theta) \right|^2 \quad (5)$$

where the a_L are the amplitudes of the Legendre polynomials P_L and φ_L corresponds to the relative phase. L_{max} is the highest partial wave considered. The amplitudes then reflect the contribution from each partial wave.

The fits to experimental data for the low (14.3–15.0 MeV) and high (15.9–16.4 MeV) ranges corresponding to the two angular distributions are given in Tables 1 and 2. What is evident from the fits to the data (Table 1) is that at low energies the fit continues to improve up to $L_{max} = 4$, whereas at the higher energy it is already converged for $L_{max} = 3$. This indicates that higher angular momenta components are important at the lower energy than at the higher energy. The angular distributions in Fig. 5 are shown with the fit corresponding to $L_{max} = 4$ and the amplitudes a_L are given in Table 2. The ratios of the amplitudes between the fits at low and high energies indicates that the $L = 4$ amplitude is the one which is most strongly enhanced at lower energies, signalling the importance of this partial wave in describing the enhanced cross section.

This behaviour is also seen from the diffractive behaviour of the angular distributions. The lower energy data, Fig. 5b, has a diffractive behaviour which sees the maximum and second minumum shift to smaller c.m. angles, similar to a Legendre polynomial of order 4. This would be consistent with an enhanced $L = 4$ contribution. Both characteristics may be traced to the additional $L = 4$ contribution. It should be noted that from an elastic scattering perspective that the opposite behaviour would be expected, i.e. higher L-values should play a stronger role at higher energy, and this points to a resonance contribution, mirroring the enhanced yield observed in Fig. 4.

It is also possible to extract from the coincidence measurements yields and angular distributions for the ^{4}He(^{8}He,^{6}He)^{6}He reaction; $Q = -1.17$ MeV. This reaction is well separated from the elastic scattering reaction by virtue of the different sum energy of the two products and the different kinematics. However, the yield is significantly smaller than that of the elastic channel. The significant background, from scattering from the window, in the coincidence spectra for the coincidences 1-1 and 1-2 meant it was not possible to unambiguously extract the ^{6}He + ^{6}He final state in those cases. However, the background for the combination 2-2 was close to zero. Fig. 6 shows the ^{6}He + ^{6}He angular distributions for these 2-2 coincidences.

For the ^{6}He + ^{6}He final-state, it is clear that the angular distributions are very different at the two excitation energies, Fig. 6a ($E_x = 15.7$ and 16.0 MeV) and Fig. 6b ($E_x = 14.4$ MeV). The angular

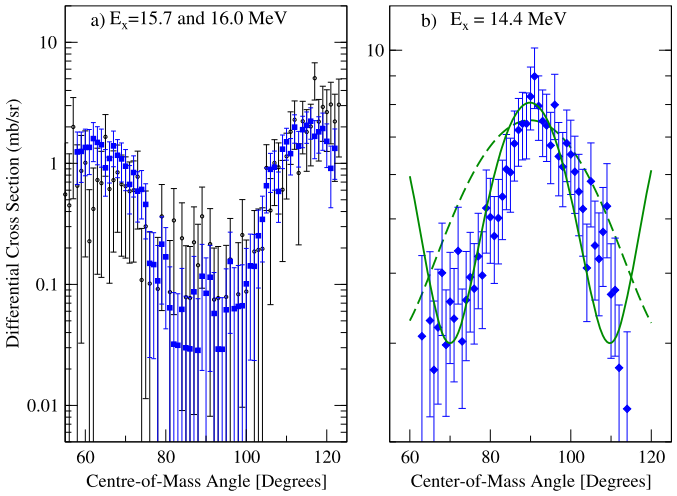

Fig. 6. (Colour online.) Angular distributions for the ^{4}He(^{8}He,^{6}He)^{6}He reaction for the excitation energy ranges a) 16.0 (blue points) and 15.7 (black points) MeV and b) 14.4 MeV (data points). The fit (red-line) corresponds to the functional form given in Eq. (5), with $L_{max} = 4$. b) additionally exhibits the oscillations of Legendre Polynomials of order 2 (dashed-green line) and 4 (solid-green line). The central maximum is characteristic of $L = 4$.

range at lower energies is limited by the detection energy threshold. At higher energies the distributions are forward-backward angle peaked, whereas at lower energy they peak at $\theta_{cm} = 90°$. Given that the final state consists of *symmetric* spin zero bosons, only the even partial waves contribute. The symmetric final state means that the angular distributions should be symmetric about 90°. It is clear that there is a stronger yield at the lower energy, both from the normalised yields shown in Fig. 4 and the differential cross sections shown in Fig. 6. It should be noted that the limited range of the angular distributions (particularly in Fig. 6b) and the limited statistics allows for a variety of fits with similar χ^2 with different partial wave amplitudes and hence unique conclusions as to the partial wave contributions could not be reached for these data. However, the narrow width of the central maximum in the angular distributions appears to be more consistent with $L = 4$ as opposed to $L = 2$ (Fig. 6b). Measurements over a wider angular range would be required to confirm these conclusions for the transfer channel.

We therefore conclude that the present data indicate that i) there are no *strong* narrow ($\sim$ 50–100 keV) ^{4}He + ^{8}He resonances in the energy intervals explored, ii) there is enhanced yield close to $E_x = 14$–15 MeV for both the reactions probed, compared with 16 MeV, and iii) this is characterised by an increased $L = 4$ component in both the elastic scattering and two-neutron transfer with a width of ~ 1 MeV or less. This would suggest that a resonance of $L = 4$ in ^{12}Be plays a role in the scattering process at this energy.

Finally, we compare in Fig. 4 the present results to the generalized two-centre cluster model (GTCM) calculations of Ito [10], which predict that 4^+ states linked to cluster or molecular structures should lie in the region 13.4 to 17.4 MeV. In particular, a strong peak in the $L = 4$ component of the ^{4}He + ^{8}He scattering cross section is predicted at $\sim$ 15.2 MeV (width $\sim$ 1.5–2 MeV), which involves the crossing of two bands with ^{6}He + ^{6}He and ^{4}He + ^{8}He structure. The present measurements agree with the calculations but suggest that this $L = 4$ strength lies at slightly lower energy and has a narrower width. Noticeably, the $L = 2$ strength in the calculations is in anti-phase with the $L = 4$ component, with the higher energy component probably lying outside the range of the present measurements. This agreement between experiment and theory suggests the molecular/cluster like structure of ^{12}Be in this excitation energy region [16]. However, it is clear that further work, both experiment and theory, is required.

In summary, the present measurements provide a high statistics determination of the angular distributions for the two reactions ^{4}He(^{8}He,^{4}He) and ^{4}He(^{8}He,^{6}He). These angular distributions and the variation in experimental yield with energy indicates a $J^\pi = 4^+$ resonance in the region $E_x = 14$–15 MeV with a width of ~ 1 MeV. The observed energy, width and spin coincide strongly with GTCM calculations that predict exotic cluster states in this region. The present measurements indicates that this ^{12}Be resonance decays to both the ^{4}He + ^{8}He and ^{6}He + ^{6}He final states. The angular distributions of the present measurements may also serve as a constraint of the validity of the generalized two-centre cluster model (GTCM) calculations and indeed an interesting test for those wishing to model the intriguing system in which the halo ^{8}He nucleus is scattered from a nucleus which is the core of the halo.

Acknowledgements

The contribution of the LPC technical staff, in particular C. Vendamme, and the GANIL operators and technical team is acknowledged.

References

[1] W. von Oertzen, M. Freer, Y. Kanada-En'yo, Phys. Rep. 432 (2006) 43.
[2] M. Freer, et al., Phys. Rev. Lett. 96 (2006) 042501.
[3] S.D. Pain, et al., Phys. Rev. Lett. 96 (2006) 032502, and references therein.
[4] Y. Kanada En'yo, H. Horriuchi, Phys. Rev. C 68 (2003) 014319.
[5] A.A. Korsheninnikov, et al., Phys. Lett. B 343 (1995) 53.
[6] M. Freer, et al., Phys. Rev. Lett. 82 (1999) 1383.
[7] R.J. Charity, et al., Phys. Rev. C 76 (2007) 064313.
[8] Z.H. Yang, et al., Phys. Rev. Lett. 112 (2014) 162501; Phys. Rev. C 91 (2015) 024304.
[9] M. Ito, N. Itagaki, H. Sakurai, K. Ikeda, Phys. Rev. Lett. 100 (2008) 182502.
[10] M. Ito, Phys. Rev. C 85 (2012) 044308.
[11] W.G. Planje, W.B. Westervald, A. Niehaus, Phys. Rev. Lett. 85 (2000) 2713.
[12] M. Freer, et al., Phys. Rev. C 90 (2014) 054324.
[13] Micron Semiconductor Ltd., 1 Royal Buildings, Marlborough Road, Churchill Industrial Estate, Lancing, Sussex BN15 8UN, UK.
[14] T. Davinson, et al., Nucl. Instrum. Methods A 454 (2000) 350.
[15] P. Darriulat, et al., Phys. Rev. 137 (1965) 315.
[16] M. Itoh, K. Ikeda, Rep. Prog. Phys. 77 (2014) 096301.